The Astrophysical Journal, 854:135 (10pp), 2018 February 20 https://doi.org/10.3847/1538-4357/aaa41e

The Genealogical Tree of Ethanol: Gas-phase Formation of Glycolaldehyde, Acetic Acid, and Formic Acid

Dimitrios Skouteris[1], Nadia Balucani[2,3,4], Cecilia Ceccarelli[3], Fanny Vazart[1], Cristina Puzzarini[4,5], Vincenzo Barone[1], Claudio Codella[4], and Bertrand Lefloch[3]
[1] Scuola Normale Superiore, Piazza dei Cavalieri 7, I-56126 Pisa, Italy; dimitrios.skouteris@sns.it
[2] Dipartimento di Chimica, Biologia e Biotecnologie, Università degli Studi di Perugia, Via Elce di Sotto 8, I-06123 Perugia, Italy; nadia.balucani@unipg.it
[3] Univ. Grenoble Alpes, CNRS, IPAG, F-38000 Grenoble, France; cecilia.ceccarelli@univ-grenoble-alpes.fr
[4] INAF-Osservatorio Astrofisico di Arcetri, Largo E. Fermi 5, I-50125, Florence, Italy
[5] Dipartimento di Chimica "Giacomo Ciamician" Università di Bologna, Via F. Selmi 2, I-40126 Bologna, Italy
Received 2017 August 14; revised 2017 December 1; accepted 2017 December 21; published 2018 February 20

Abstract

Despite the harsh conditions of the interstellar medium, chemistry thrives in it, especially in star-forming regions where several interstellar complex organic molecules (iCOMs) have been detected. Yet, how these species are synthesized is a mystery. The majority of current models claim that this happens on interstellar grain surfaces. Nevertheless, evidence is mounting that neutral gas-phase chemistry plays an important role. In this paper, we propose a new scheme for the gas-phase synthesis of glycolaldehyde, a species with a prebiotic potential and for which no gas-phase formation route was previously known. In the proposed scheme, the ancestor is ethanol and the glycolaldehyde sister species are acetic acid (another iCOM with unknown gas-phase formation routes) and formic acid. For the reactions of the new scheme with no available data, we have performed electronic structure and kinetics calculations deriving rate coefficients and branching ratios. Furthermore, after a careful review of the chemistry literature, we revised the available chemical networks, adding and correcting several reactions related to glycolaldehyde, acetic acid, and formic acid. The new chemical network has been used in an astrochemical model to predict the abundance of glycolaldehyde, acetic acid, and formic acid. The predicted abundance of glycolaldehyde depends on the ethanol abundance in the gas phase and is in excellent agreement with the measured one in hot corinos and shock sites. Our new model overpredicts the abundance of acetic acid and formic acid by about a factor of 10, which might imply a yet incomplete reaction network.

Key words: ISM: abundances – ISM: molecules

1. Introduction

About one-third of the ∼200 molecules detected in the interstellar medium (ISM) are constituted by six or more atoms.[6] All of these molecules contain at least one carbon atom. In the following, we will call molecules with at least six atoms and containing at least one carbon atom interstellar complex organic molecules (iCOMs[7]). In the majority of iCOMs, hydrogen and oxygen are the additional elements. To date, slightly more than 40 iCOMs that contain elements other than C and H have been detected. Thus, they represent about 20% of detected ISM molecules.

Even though the presence of iCOMs has been known for decades (for instance, formamide has been detected by Rubin et al. 1971), the processes that lead to their synthesis are still hotly debated. Specifically, it is currently often assumed that iCOMs are mostly synthesized on grain surfaces during the so-called warm-up phase, when various radicals trapped in the grain mantles acquire mobility and recombine into large molecules (e.g., Garrod & Herbst 2006; Garrod et al. 2008). Yet, recent detections of iCOMs in cold environments (Bacmann et al. 2012; Cernicharo et al. 2012; Jaber et al. 2014; Vastel et al. 2014; Jiménez-Serra et al. 2016) have challenged this exclusive role of grain-surface chemistry. Clearly, some gas-phase chemistry is at work in cold environments (Vasyunin & Herbst 2013; Balucani et al. 2015; Ruaud et al. 2016; Vasyunin et al. 2017).

Supporting the idea that grain-surface chemistry cannot synthesize all detected iCOMs, recent quantum chemistry calculations have shown that the combination of radicals trapped in amorphous water ice does not necessarily lead to larger molecules (Enrique-Romero et al. 2016; Rimola et al. 2017), in particular, to iCOMs, as predicted by the above-mentioned grain-surface chemical models. The basic reason is that radicals are not oriented in a way for the recombination reaction to occur, as they are trapped by the water-ice molecules in a configuration that favors other two-product reactions.

Following up with the idea that gas-phase reactions might have been overlooked, Kahane et al. (2013) proposed that formamide (NH_2CHO) is formed by the reaction of formaldehyde (H_2CO) and amidogen (NH_2). Barone et al. (2015), Vazart et al. (2016), and Skouteris et al. (2017) carried out theoretical computations showing that this reaction can efficiently occur at low temperatures (contrary to what was claimed by Song & Kästner 2016) and can explain the available observations. Other studies have explored possible gas-phase

[6] http://www.astro.uni-koeln.de/cdms/molecules
[7] Please note that we added "i" to the commonly used COMs acronym in order to be clear that these molecules are only complex in the interstellar context (Ceccarelli et al. 2017), contrary to what chemists would consider complex in the terrestrial context.

ion–neutral reactions leading to formamide (Spezia et al. 2016). More recently, an observational study obtained with the IRAM-NOEMA interferometer provided additional support to the gas-phase formation of formamide (Codella et al. 2017). Similarly, observations of its deuterated forms by Coutens et al. (2016) are in good agreement with the theoretical predictions of deuterated amidogen or formaldehyde leading to deuterated formamide (Skouteris et al. 2017).

In summary, it is well possible that gas-phase reactions play an important role in the formation of iCOMs, but more systems need to be studied to understand their real importance.

The aim of this paper is to understand whether previously overlooked gas-phase routes can lead to glycolaldehyde ($HCOCH_2OH$), a "special" iCOM because of its prebiotic potential. Glycolaldehyde has been detected toward the giant molecular cloud complex SgrB2 (Hollis et al. 2000), toward high- and low-mass star-forming regions (Béltran et al. 2009; Jørgensen et al. 2012, 2016; Coutens et al. 2015; Taquet et al. 2015; De Simone et al. 2017) and in shocked regions (Lefloch et al. 2017). Several mechanisms of glycolaldehyde synthesis on grain surfaces were proposed: they involve recombination of radicals (Garrod et al. 2008), UV, or particle irradiation (Woods et al. 2012; Maity et al. 2014; Butscher et al. 2015, 2016; Fedoseev et al. 2015; Chuang et al. 2017). On the contrary, previous work on glycolaldehyde formation in the gas phase could not identify plausible interstellar routes (Wang & Bowie 2010; Jalbout 2007).

In a recent work, Lefloch et al. (2017) showed that there is a correlation between the abundances of glycolaldehyde and ethanol, even though this is based on only four sources. Following the suggestion provided by this possible correlation, in this work we propose a series of gas-phase reactions that start from ethanol (CH_3CH_2OH) and that lead to the synthesis of glycolaldehyde in a sequence of gas-phase reactions that is similar to that connecting dimethyl ether and methyl formate, two other common iCOMs (Balucani et al. 2015). As in that case, the sequence of reactions starts with the conversion of ethanol (or its isomer dimethyl ether in the case analyzed by Balucani et al. 2015) to a reactive radical that can further react with abundant O atoms leading to glycolaldehyde (methyl formate in the case analyzed by Balucani et al. 2015). Some of the necessary data to test this hypothesis were available in the literature (see Section 3). Some crucial data were instead missing. Therefore, to verify whether the proposed route is efficient in the ISM conditions, we have performed dedicated electronic structure and kinetics calculations for the missing reactions. The main result of this work is that ethanol can be considered not only the ancestor of glycolaldehyde, but also of formic acid (HCOOH) and acetic acid (CH_3COOH), another common iCOM. In addition, ethanol is revealed to be one of the precursors of acetaldehyde, a widely spread iCOM. In other words, ethanol can be considered the progenitor of three iCOMs and of formic acid.

The article is organized as follows. In Section 2, we briefly review the previously known gas-phase reactions of the above iCOMs and formic acid. We then present the overall scheme and justification of the newly proposed reactions in Section 3 and the employed methodology and results of our computations in Section 4. In Section 5, we present the predictions obtained by an astrochemical model including the new reactions, and we discuss the comparison with observations. Section 6 concludes this article.

2. Previous Gas-phase Reactions Leading to Glycolaldehyde, Acetic Acid, Formic Acid, and Acetaldehyde

In this section, we briefly review the gas-phase reactions forming glycolaldehyde, acetic acid, formic acid, and acetaldehyde, listed in the publicly available chemical databases, KIDA[8] (Wakelam et al. 2015) and UMIST[9] (McElroy et al. 2013), and in the literature.

2.1. Glycolaldehyde ($HCOCH_2OH$)

No reactions are reported in the KIDA or UMIST databases. Halfen et al. (2006) proposed that protonated formaldehyde (H_2COH^+) could react with formaldehyde to produce protonated glycolaldehyde in a radiative association reaction. The electron recombination of protonated glycolaldehyde then ends in glycolaldehyde by losing an H atom. However, electronic structure calculations by Horn et al. (2004) showed that the relative association products do not have the molecular structure of protonated glycolaldehyde. Furthermore, it has been known since the experimental work by Karpas & Klein (1975) that two-product exothermic channels are available for the $H_2COH^+ + H_2COH$ reaction, which strongly reduces the probability of radiative association in the absence of secondary collisions. Finally, Woods et al. (2012, 2013) claimed that this route is inefficient and cannot reproduce the observed abundances.

2.2. Acetic Acid (CH_3COOH)

No reactions are reported in the KIDA or UMIST databases for this species, and we are not aware of proposed schemes of its formation in the gas phase.

2.3. Formic Acid (HCOOH)

KIDA lists one reaction, $CH_3O_2^+ + e^-$, which is assumed to produce 50% of HCOOH (+ H) and 50% of CO_2 (+ H_2 + H). In UMIST, the same reaction, reported as $HCOOH_2^+ + e^-$, is globally faster, but has a branching ratio of only 13% for the HCOOH channel, with the major channel leading to HCO + OH + H. The UMIST rate coefficients are based on the experiments by Vigren et al. (2013), who were, however, only able to demonstrate that heavy products with at least one C and two O atoms account for 13% of the global reaction. This could include also CO_2 formation, as suggested in KIDA. In addition to that, there are issues concerning the formation of the $HCOOH_2^+$ / $CH_3O_2^+$ isomers. The main formation route of so-called protonated formic acid is considered to be the radiative association reaction $HCO^+ + H_2O$ (Herbst 1985). In the KIDA and UMIST networks, this process is present with a relatively high rate coefficient of 1.7×10^{-12} cm^3 s^{-1} at 100 K. In general, the rate coefficients of most radiative association reactions are poorly defined and can only be estimated. From what is known so far, a significant probability for radiative association reactions to occur can be expected only when there are no exothermic two-product channels or when the presence of

[8] http://kida.obs.u-bordeaux1.fr
[9] http://udfa.ajmarkwick.net

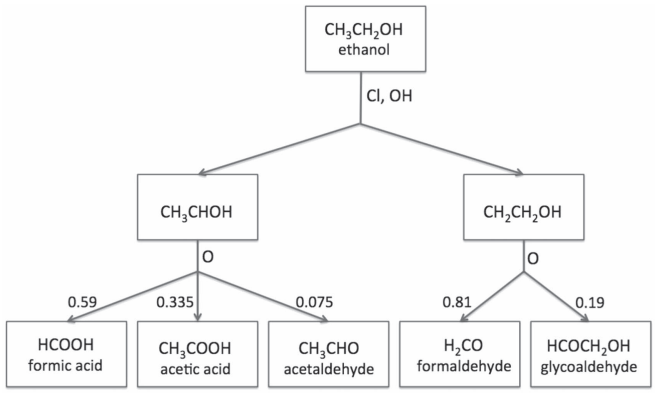

Figure 1. Scheme of the reactions starting from ethanol. The numbers indicate the relative branching ratios (see the text).

very high exit barriers prevents a fast escape from the potential well associated with the addition intermediate. Only in these cases, can the lifetime of the intermediate indeed be long enough to permit the spontaneous emission of photons necessary for its stabilization (in the absence of ternary collisions, as in interstellar environments). As warned by Herbst (1985), this is not the case for the $HCO^+ + H_2O$, which is indeed a fast reaction (3.64×10^{-9} cm^3 s^{-1} at 100 K) with a very exothermic two-product channel (leading to $CO + H_3O^+$). For this reason, we have deleted the radiative association of $HCO^+ + H_2O$ from our reaction network. The other routes of $HCOOH_2^+/CH_3O_2^+$ formation have already been proved to be marginal (Vigren et al. 2013). In addition, UMIST also reports $OH + H_2CO \rightarrow HCOOH + H$, a reaction that has been widely studied at higher temperatures. Since the channel leading to HCOOH + H has an entrance barrier of 23.8 kJ/mol (Xu & Lin 2007), we did not consider it in our network. Other reactions listed in UMIST are expected to make a negligible contribution to HCOOH formation.

2.4. Acetaldehyde (CH_3CHO)

Several reactions forming acetaldehyde are reported in KIDA. A possibly major formation route is the electron recombination of protonated acetaldehyde that ends up in acetaldehyde. However, the protonated acetaldehyde is mostly formed by the reaction $CH_3OCH_3 + H^+ \rightarrow CH_3CHOH^+ + H_2$, which would imply a substantial and improbable rearrangement of the nuclei. Therefore, we dropped this reaction from the network. Another major formation reaction route, and often the most important one in several published models, involves atomic oxygen and ethyl radical: $CH_3CH_2 + O \rightarrow CH_3CHO + H$ (Charnley 2004; Vastel et al. 2014; Codella et al. 2015).

3. New Reaction Scheme

Figure 1 illustrates the scheme of the reactions proposed in this work.

In the proposed new reaction scheme, ethanol is chemically activated by one of the abundant atomic or molecular radicals that are present in interstellar clouds. In Balucani et al. (2015), several radicals were considered and atomic chlorine was suggested as the major contributor in converting dimethyl ether into the reactive methylmethoxy radical. Vasyunin et al. (2017) considered, instead, that the abundant OH radicals are the major players by referring to the recent work by Shannon et al. (2014), who performed kinetics experiments at T as low as 60 K.[10]

We follow the same approach here, that is, we have considered the reaction of ethanol with Cl atoms and OH radicals as the initiating steps. In the following, we give details of the employed reactions.

3.1. The Initiating Reaction $Cl + CH_3CH_2OH$

This reaction has been widely investigated at room or higher temperatures. In particular, Taatjes et al. (1999) were able to derive the H-abstraction site-specific rate coefficients as, unlike the case of dimethyl ether, three different kinds of hydrogen atoms that Cl (or other radicals) can abstract: (i) three equivalent H-atoms from the methyl group (CH_3), (ii) two equivalent H-atoms from the methylene group (CH_2), and (iii) one H atom from the hydroxyl group (OH). According to the measurements by Taatjes et al. (1999) at room temperature, H-abstraction from the methylene group (ii) is by far the dominant pathway accounting for about 90% of the total reaction. H-abstraction from the methyl group (i) accounts for the rest, while abstraction of the hydroxyl hydrogen (iii) is negligible. Unfortunately, there are no experimental data at the low temperatures of interest in our case. Therefore, in our network we have included the reaction channels (labeled reactions 1 and 2 in Table 1) with their room-temperature values. In addition, the product branching ratio for the reaction $Cl + CH_3CH_2OH$ could slightly vary with the temperature as channel (1) is exothermic by 44.8 kJ/mol and channel (2) by 17.6 kJ/mol, while the channel leading to CH_3CH_2O is slightly endothermic by 3.8 kJ/mol (Rusic & Berkowitz 1994). Moreover, electronic structure calculations by Rudic et al. (2002) predicted a very small barrier of *ca. 3* kJ/mol for channel (2).

3.2. The Initiating Reaction $OH + CH_3CH_2OH$

This reaction has been widely investigated at room or higher temperatures and, more recently, also at temperatures as low as 50 K by Caravan et al. (2015). Similarly to the case of the analogous reaction with dimethyl ether in low-temperature experiments, the observed pressure dependence of the rate coefficients provided evidence that, in addition to the bimolecular abstraction channel leading to products, collisional stabilization of the weakly bound OH-ethanol complex occurred under their experimental conditions—thus providing an artificially high rate coefficient (we note that such a mechanism cannot be present under the rarefied conditions of the interstellar medium). In our network, we have considered the value of the rate coefficient that Caravan et al. (2015) recommended as representative of the sole two-product channel, that is, at 82–91 K, $2.7\ (\pm 0.8) \times 10^{-11}$ cm^3 s^{-1}. Also in this case, the H-abstraction can occur at three different sites, leading to the radicals CH_2CH_2OH, CH_3CHOH, and CH_3CH_2O. As CH_3O (+ H_2O) was determined to be the major product in the analogous reaction $OH + CH_3OH$ by Shannon et al. (2013), Caravan et al. (2015) attempted the detection of CH_3CH_2O, but failed. At higher T, the formation of CH_3CHOH (+ H_2O) is known to be the main channel, with a branching

[10] We would like to note, however, that the most appropriate value for the rate coefficient of the bimolecular reaction leading to $CH_3OCH_2 + H_2O$ is about one-half of that quoted by Vasyunin et al. (2017) because of the pressure dependence noted and discussed by Shannon et al. (2014) in their work.

Table 1
List of the Reactions of the Proposed Scheme to Form Glycolaldehyde and Acetic Acid from Ethanol

Reaction	α	β	γ	Label	Notes
$CH_3CH_2OH + Cl \rightarrow CH_3CHOH + HCl$	9.8(−11)	0	0	1	1
$CH_3CH_2OH + Cl \rightarrow CH_2CH_2OH + HCl$	1.1(−11)	0	0	2	1
$CH_3CH_2OH + OH \rightarrow CH_3CHOH + H_2O$	2.4(−11)	0	0	3a	2
$CH_3CH_2OH + OH \rightarrow CH_3CHOH + H_2O$	1.9(−11)	0	0	3b	2
$CH_3CH_2OH + OH \rightarrow CH_2CH_2OH + H_2O$	2.7(−12)	0	0	4a	2
$CH_3CH_2OH + OH \rightarrow CH_2CH_2OH + H_2O$	8.1(−12)	0	0	4b	2
$CH_3CHOH + O \rightarrow HCOOH + CH_3$	3.9(−10)	0.18	0.49	5	3
$CH_3CHOH + O \rightarrow CH_3CHO + OH$	4.8(−11)	0.19	0.39	6	3
$CH_3CHOH + O \rightarrow CH_3COOH + H$	2.2(−10)	0.16	0.59	7	3
$CH_2CH_2OH + O \rightarrow HCOCH_2OH + H$	1.1(−10)	0.16	0.55	8	3
$CH_2CH_2OH + O \rightarrow H_2CO + CH_2OH$	4.6(−10)	0.17	0.51	9	3

Note. α, β, and γ are the coefficients for the rate constants, computed according to the usual equation $k = \alpha \times (T_{gas}/300\ K)^{\beta} \times \exp[-\gamma/T_{gas}]$. The last two columns report the reaction labels and notes. (1) We have used the (rounded) values at 300 K measured by Taatjes et al. (1999). (2) We have adopted the total value measured by Caravan et al. (2015) in the range 82−91 K, partitioned according to two possible scenarios for channels 3 and 4 (see the text). (3) The rate coefficients and product branching ratios are those computed in the present work.

ratio varying between 0.75 and 0.9, while the CH_2CH_2OH (+ H_2O) channel accounts for the rest (Marinov 1999; Carr et al. 2011). The branching ratio was also seen to vary with T. We have, therefore, decided to test two different scenarios: in the first scenario, we have assumed a value of 0.9:0.1 (reactions 3a and 4a in Table 1); in the second scenario, we have assumed a value of 0.7:0.3 (reactions 3b and 4b in Table 1). Even though these seem to be reasonable ranges, a final value could be adopted only when low T determination of the branching ratio becomes available.

3.3. Second Step: Reactions of CH_3CHOH and CH_2CH_2OH with O

Further reactions of the radicals produced in the initiating steps with atomic oxygen generate the species shown in Figure 1. To the best of our knowledge, only fragmentary data were available in the literature concerning the reaction channel $O + CH_3CHOH \rightarrow CH_3CHO + OH$ (Edelbüttel-Einhaus et al. 1992), so we have performed dedicated electronic structure and kinetics calculations. The results of the calculations are reported in Section 4. The resulting overall picture is that CH_3CHOH and CH_2CH_2OH can form (i) starting from CH_3CHOH formic acid (59%), acetaldehyde (7.5%), acetic acid (33.5%), and (ii) starting from CH_2CH_2OH glycolaldehyde (19%) and H_2CO (81%), respectively.

The reactions with their branching ratios and rate coefficients are reported in Table 1.

4. Computational Details and Results

4.1. Electronic Structure Calculations

Calculations have been performed with a development version of the Gaussian suite of programs (Frisch et al. 2013) as well as with the CFOUR program package.[11] Geometry optimizations for all stationary points were performed with the double-hybrid B2PLYP functional (Grimme 2006) in conjunction with the m-aug-cc-pVTZ basis set (Papajak et al. 2009; Dunning 1989), where d functions on hydrogens have been removed. Semi-empirical dispersion contributions were also included by means of the D3BJ model of Grimme (Goerigk & Grimme 2011; Grimme et al. 2011). Full geometry optimizations have been performed for all molecules checking the nature of the obtained structures (minima or first-order saddle points) by diagonalizing their Hessians. For each stationary points, the anharmonic force field has been computed at the B2PLYP-D3BJ/m-aug-cc-pVTZ level in order to evaluate the zero-point energies (ZPEs) using vibrational perturbation theory (VPT2). To obtain accurate electronic energies, the coupled-cluster singles and doubles approximation augmented by a perturbative treatment of triple excitations (CCSD(T); Raghavachari et al. 1989) was employed in conjunction with extrapolation to the complete basis set limit (CBS) and inclusion of core-correlation effects (CV), thus leading to the so-called CCSD(T)/CBS+CV approach (Heckert et al. 2005, 2006). The cc-pVnZ, with $n = T$, Q, basis sets (Dunning 1989) were used in the extrapolation to the CBS limit, while the cc-pCVTZ set (Woon & Dunning 1995) was employed for evaluating the CV correction.

4.2. Reaction Paths for the Reactions $O + CH_2CH_2OH$ and $O + CH_3CHOH$

The reaction paths for both schemes are shown in Figures 2, 3.

Figure 2 exhibits the reaction path following the $O(^3P) + CH_2CH_2OH$ addition. The barrierless addition of oxygen leads to the (I) intermediate, which is about 400 kJ/mol more stable than the reactants. Its *trans* counterpart, the slightly less stable (by 8 kJ/mol) intermediate (II), can easily be reached from the *cis* species through a 20 kJ/mol barrier (TS1). Both intermediates are then able to undergo dissociation to formaldehyde and CH_2OH through the transition states (TS6) and (TS5). These dissociations exhibit barriers around 55 kJ/mol. Other dissociations can also be observed from both these intermediates, leading to *cis*- or *trans*-glycolaldehyde and H, respectively, through (TS2) and (TS3) that are about 115 kJ/mol higher in energy than their corresponding dissociating intermediates. The most stable products that can be obtained with this path

[11] CFOUR, a quantum chemical program package written by J. F. Stanton, J. Gauss, M. E. Harding, and P. G. Szalay with contributions from A. A. Auer, R. J. Bartlett, U. Benedikt et al. and the integral packages MOLECULE (J. Almlöf & P. R. Taylor), PROPS (P. R. Taylor), ABACUS (T. Helgaker, H. J. Aa. Jensen, P. Jørgensen, & J. Olsen), and ECP routines by A. V. Mitin & C. van Wüllen. For the current version, see http://www.cfour.de).

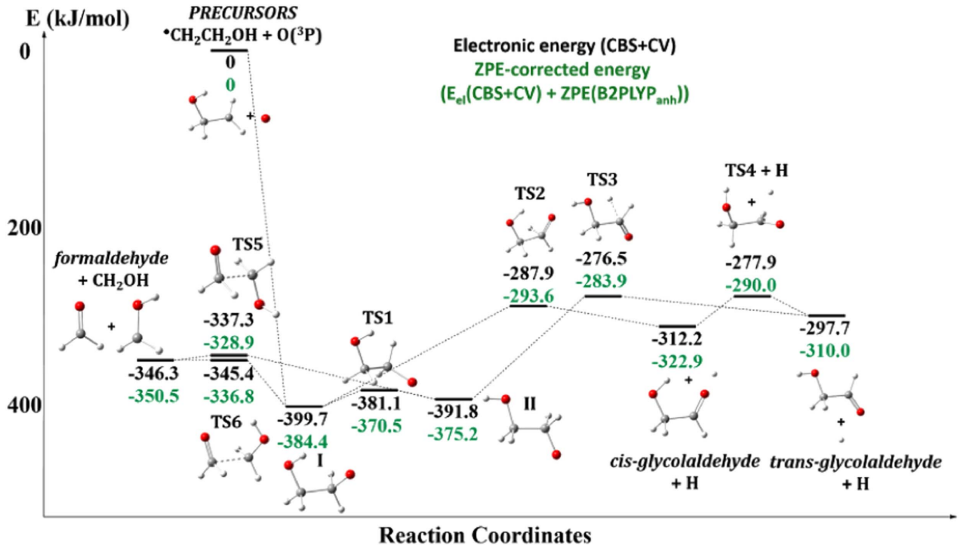

Figure 2. Reaction path for the $O(^3P) + CH_2CH_2OH$ scheme. Both electronic (above) and zero-point-corrected (below) energies are shown.

are formaldehyde + CH_2OH, with a relative energy of around −346 kJ/mol followed by the glycolaldehyde isomers, with a relative energy of around −310 kJ/mol.

Wang & Bowie (2010) performed electronic structure calculations for the same global potential energy surface, but considered the possible formation of glycolaldehyde from the reaction $H_2CO + CH_2OH$. Their entrance channel, therefore, is one of the exit channels in our case. The energy values of the corresponding intermediates and transition states can be compared and are in general good agreement. More specifically, our values for the energy of the transition states and global endothermicity are lower than the ones presented in that work. Nevertheless, both are still high enough to render the reaction $H_2CO + CH_2OH \rightarrow HCOCH_2OH + H$ prohibitive in the ISM.

Figure 3 exhibits the reaction path following the $O(^3P) + CH_3CHOH$ addition. The barrierless addition of oxygen leads to the (III) intermediate, which is about 410 kJ/mol more stable than the reactants. This species is then able to undergo a dissociation into formic acid and the CH_3 radical, through the (TS11) transition state. This dissociation exhibits an approximate 45 kJ/mol barrier. Another dissociation can also be observed, leading to acetic acid and H, through (TS9) which is about 60 kJ/mol higher in energy than (III). Starting again from (III), elimination of an OH radical can occur (through the (TS8) transition state, lying approximately 100 kJ/mol above the intermediate), yielding acetaldehyde. Furthermore, from (III) hydrogen migration can lead to compound (IV) with a barrier of 105 (TS7) kJ/mol. The intermediate (IV) is found to be around 460 kJ/mol more stable than the precursor. (IV) can also undergo hydrogen loss resulting in acetic acid and H through a 117 kJ/mol barrier (TS10). The most stable products are formic acid and CH_3, with a relative energy of −419.5 kJ/mol with respect to the precursors, followed by acetic acid + H that exhibits a relative energy of −395.3 kJ/mol.

4.3. Kinetics Calculations

As in previous work (Balucani et al. 2012; Leonori et al. 2013; Skouteris et al. 2015; Vazart et al. 2015; Sleiman et al. 2017) a combination of capture theory and the Rice-Ramsperger-Kassel-Marcus (RRKM) calculations was used to determine the relevant rate coefficients and branching ratios. For the first steps (addition of the $O(^3P)$ atom to either the CH_2CH_2OH or the CH_3CHOH radicals) capture theory was used, whereas for the subsequent reactions energy-dependent rate constants were calculated using the RRKM scheme and taking into account anharmonicity of the vibrational modes. Subsequently, the master equation was solved at all relevant energies for both systems (to take into account the overall reaction scheme), Boltzmann averaging was carried out to obtain temperature-dependent rate coefficients, and finally, rate coefficients were fitted to the form $k = \alpha \times (T_{gas}/300\,K)^{\beta} \times \exp[-\gamma/T_{gas}]$. The values of α, β, and γ in each case are given in Table 1.

Back-dissociation is negligible in both cases, due to the high stability of the initial intermediate and the presence of very exothermic channels with low exit energy barriers. When the O atom adds to CH_2CH_2OH, the most probable fates of the radical are cleavage of the C–C bond (to yield formaldehyde and the CH_2OH radical) or an H atom elimination to give glycolaldehyde. The first one dominates at all temperatures due to the significantly lower energy barrier involved. Nevertheless, as can be seen from the final values, a substantial percentage of the intermediate goes to glycolaldehyde (yield of 19%).

An analogous situation presents itself when the O atom adds to the CH_3CHOH radical. The two most probable fates of the addition intermediate are C–C bond cleavage, yielding HCOOH and a methyl radical, and elimination of an H atom from the α C atom to yield acetic acid (CH_3COOH). Before the elimination, there is also the possibility of an H atom transfer from the α C atom to the newly added oxygen, followed by an H atom elimination from one of the two O atoms. However, this is the least followed path toward acetic acid formation, both because of the higher barrier involved and the longer reaction path. The most abundant product is formic acid (with a yield of 59%), because of the lower barrier involved, while acetic acid formation is second highest (33.5%). Finally, there is some possibility of elimination of an OH radical from the initial intermediate, yielding CH_3CHO. The barrier for this process is considerably higher than both previous ones, and therefore the rate of formation of acetaldehyde is lower.

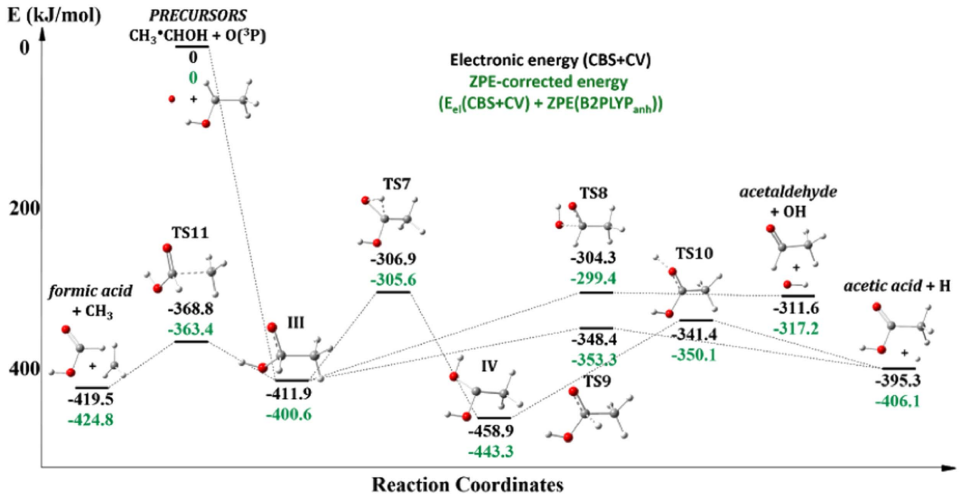

Figure 3. Reaction path for the $O(^3P) + CH_3CHOH$ scheme. Both electronic (above) and zero-point-corrected energies (below) are shown.

Concerning this last point, it should be noted that Edelbüttel-Einhaus et al. (1992) were, instead, only able to detect the CH_3CHO product in their room-temperature experiments.

5. Astrochemical Modeling

5.1. Description of the Model

In order to understand whether the proposed new reaction scheme and rate coefficients can explain observations toward hot corinos, we used an astrochemical model which simulates their conditions. Toward this scope, we used a modified version (to improve its versatility) of the time-dependent chemistry code NAHOON.[12] We run the code in two steps. In the first step, we follow the chemical composition of the molecular cloud from which the hot corino evolves. We start with the standard atomic state with the element abundances listed in Table 2 and wait for the steady state composition of the gas. We then simulate the hot corino appearance by injecting into the gas phase the species previously frozen into the dust grain mantles in the quantities listed in Table 2. The assumption is that when the dust grain temperature reaches ∼100 K the ice mantles sublimate and all species trapped in the water matrix co-desorb with it. This is a rough approximation, but enough for the scope of this article, the aim of which is to provide an order of magnitude of the species abundances.

The starting point of our proposed chemical scheme is the sublimation of ethanol from interstellar grains. Since IR observations have (only) possibly identified this species in the ice mantles of interstellar grains (Schutte et al. 1999; Oberg et al. 2011; Boogert et al. 2015), its abundance is a parameter of the model, which we varied between 10^{-8} and 10^{-6}.

Similarly, it is not clear what the abundance of atomic chlorine in hot corinos is. On Earth, chlorine is mostly in oceans and very little in rocks. Therefore, only a small fraction of chlorine is probably contained in the refractory grains of the ISM (Jenkins 2009). Observations of HCl in hot cores/corinos and shock sites show that this molecule has an abundance of $\sim 10^{-9}$ (e.g., Peng et al. 2010; Codella et al. 2012; Kama et al. 2015), namely, about 300 times lower than the solar abundance. Since in hot cores/corinos and shock sites the grain mantles components are injected into the gas phase, these observations show that HCl is not the major reservoir of chlorine, contrary to model predictions (e.g., Neufeld et al. 2012). It is, therefore, possible, if not likely, that a large fraction of Cl is atomic. Since no observations exist to constrain the abundance of atomic chlorine in hot corinos, its abundance is considered a parameter of the model and it is varied between 10^{-9} and 10^{-7}. The highest value corresponds

[12] The original code is publicly available at http://kida.obs.u-bordeaux1.fr (Wakelam 2014).

Table 2
List of the Species Injected from the Iced Mantles (Step 2), plus the Elemental Abundances of the Molecular Cloud Phase (Step 1)

Species	Abundance
Step 1: Elemental Abundances	
He	9.0×10^{-2}
O	2.6×10^{-5}
C	1.7×10^{-5}
N	6.2×10^{-6}
S	8.0×10^{-8}
Si	8.0×10^{-9}
Mg	7.0×10^{-9}
Fe	3.0×10^{-9}
Na	2.0×10^{-9}
Cl	1.0×10^{-9}
F	1.0×10^{-9}
Step 2: Injected Mantle Species	
H_2O	1.0×10^{-4}
CO	2.0×10^{-5}
CO_2	2.0×10^{-5}
H_2CO	5.0×10^{-6}
CH_3OH	5.0×10^{-6}
NH_3	5.0×10^{-6}
CH_4	3.0×10^{-6}
CH_3CH_2OH	1.0×10^{-8}–1.0×10^{-6}
Cl	1.0×10^{-9}–1.0×10^{-7}

Note. The abundances of the injected species are taken from Boogert et al. (2015), who give them relative to H_2O. The elemental abundances are 5% of the solar ones for oxygen, carbon, and nitrogen, and 0.5% for the heavier elements to account for the freeze-out of these elements in the molecular cloud. Please note that the Cl abundance is a parameter of the model (see the text). All abundances are with respect to H-atoms.

Table 3
List of New Reactions Added to the Chemical Network

Reaction	α	β	γ	Label	Notes
$HCOCH_2OH + HX^+ \rightarrow HCOCH_2OH_2^+ + X$	2.0(−9)	0	0	10	1
$HCOCH_2OH + He^+ \rightarrow HCO^+ + CH_2OH + He$	1.0(−9)	0	0	11	2
$HCOCH_2OH + H^+ \rightarrow HCO^+ + CH_2OH + H$	1.0(−9)	0	0	12	2
$CH_3COOH + HCO^+ \rightarrow CH_3CO^+ + CO + H_2O$	2.5(−9)	0	0	13	3
$CH_3COOH + H_3^+ \rightarrow CH_3CO^+ + H_2 + H_2O$	6.8(−9)	0	0	14	3
$CH_3COOH + H_3O^+ \rightarrow CH_3CO^+ + H_2O + H_2O$	2.6(−9)	0	0	15	3
$CH_3COOH + H^+ \rightarrow CH_3CO^+ + H_2O$	7.4(−9)	0	0	16	3
$CH_3COOH + He^+ \rightarrow CH_3CO^+ + OH + He$	4.0(−9)	0	0	17	3
$CH_2CH_2OH/CH_3CHOH + HX^+ \rightarrow CH_3CH_2OH^+ + X$	2.0(−9)	0	0	18	4
CH_2CH_2OH / $CH_3CHOH + H^+ \rightarrow CH_3CHOH^+ + H$	3.0(−9)	−0.5	0	19	5
CH_2CH_2OH / $CH_3CHOH + He^+ \rightarrow C_2H_4^+ + OH + He$	3.0(−9)	−0.5	0	20	6
$HCOCH_2OH_2^+ + e \rightarrow HCOCH_2OH + H$	1.5(−7)	−0.5	0	21	7
$CH_3CHOH^+ + e \rightarrow H_2CO + CH_3$	8.5(−7)	−0.74	0	22	8
$CH_3CHOH^+ + e \rightarrow H + H_2CO + CH_2$	8.5(−7)	−0.74	0	23	8
$CH_3CHOH^+ + e \rightarrow H + HCO + CH_3$	8.5(−7)	−0.74	0	24	8
$CH_3CHOH^+ + e \rightarrow H + CO + CH_4$	8.5(−7)	−0.74	0	25	8
$CH_3CHOH^+ + e \rightarrow H + CH_3CHO$	3.0(−7)	−0.74	0	26	8

Note. Notes on each reaction are reported in the Appendix.

to the assumption that 70% of Cl is depleted in the refractory grains or in other Cl- bearing molecules.

The other crucial species involved in the initiating steps of the proposed scheme is OH (Table 1). This radical is a product of the injection of water from the ice mantles and it is self-consistently computed by the astrochemical model. In this case, we adopted the "standard" value for injected water of 1×10^{-4} (e.g., Boogert et al. 2015), as quoted in Table 2.

Finally, the H density of the hot corinos is assumed to be 2×10^8 cm^{-3} and its temperature is 100 K. The cosmic-ray ionization rate is assumed to be 3×10^{-16} s^{-1} (e.g., Caselli & Ceccarelli 2012).

5.2. Chemical Network

We used the KIDA network,[13] modified following Loison et al. (2014), Balucani et al. (2015), and Skouteris et al. (2017), plus the reactions in Tables 1 and 3. The first table reports the reactions in the new proposed scheme (Section 3), whereas the second table lists the reactions added to complete the formation and destruction routes of the newly introduced species (i.e., not present in the KIDA database) or the reactions that were modified with respect to the KIDA content. Notes with the relevant references and arguments are listed in the Appendix.

We emphasize that the first step, which leads to CH_3CHOH and CH_2CH_2OH from ethanol, can be obtained either via the reaction with atomic Cl or OH. Since in the literature there have been different values of branching ratios for the latter reaction, we considered two different scenarios (see Section 3), namely, the two sets of reactions (3a), (4a) and (3b), (4b), respectively.

5.3. Results

We run three grids of models, each with the abundance of injected ethanol and atomic chlorine in the range reported in Table 2. The three grids are obtained by varying the conditions of the initiating steps of our proposed scheme (Figure 1), namely, the reactions of Table 1 numbered 1 to 4. In the first grid, we adopted the rates of (3a) and (4a), in the second grid the rates of (3b) and (4b), and in the last grid we did not consider reactions (3) and (4) to quantify the role of atomic chlorine.

The results at 1.5×10^3 years (the approximate age of hot corinos and of L1157-B1) are shown in Figure 4. The figure shows the abundance of glycolaldehyde as a function of the ethanol abundance in the gas, which can be different from the one injected from the mantles (as it is used to make the other species). We predict glycolaldehyde abundances in the range of 3×10^{-10} to 2×10^{-8} and ethanol from 10^{-9} to 10^{-7}. The largest glycolaldehyde abundances are obtained adopting the most favorable branching ratio of the reaction between ethanol

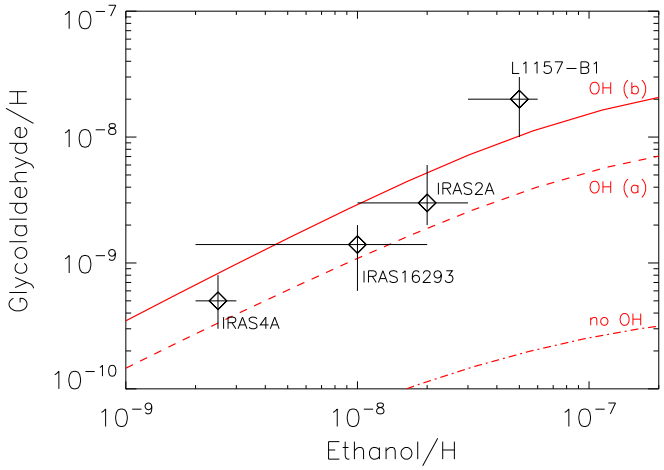

Figure 4. Abundance of glycolaldehyde as a function of ethanol abundance in the gas phase, which can be different from the one injected from the mantles. The computations refer to a gas with a temperature equal to 100 K, H nuclei density 2×10^8 cm^{-3}, cosmic-ray ionization rate 3×10^{-1} s^{-1}, and time 1.5×10^3 years. The three curves refer to models with different reactions of Table 1: adopting reactions (3b) and (4b) (solid line), reactions (3a) and (4a) (dashed line), and excluding the reaction with the OH radicals (dotted–dashed line). The atomic chlorine abundance is 2.2×10^{-8} in the computations. Measured abundances toward NGC 1333, IRAS 4A and IRAS 2A, IRAS 16293-2422, and L1157-B1 are also reported with their uncertainties.

[13] The original network is publicly available at http://kida.obs.u-bordeaux1.fr (Wakelam et al. 2015).

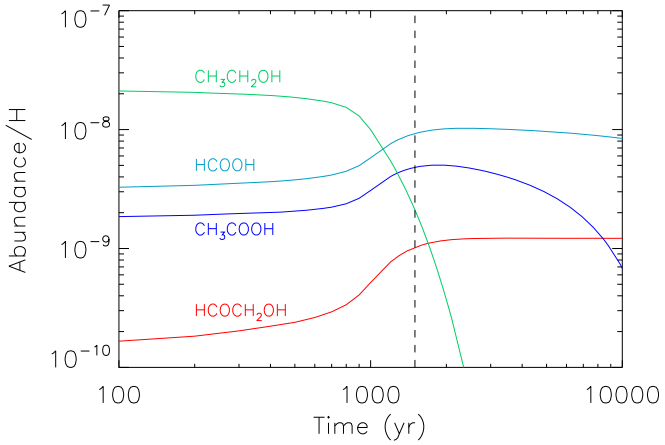

Figure 5. Abundance of glycolaldehyde (red), acetic acid (purple), formic acid (cyan), and ethanol (green) as a function of time. The computations are obtained for a gas with temperature equal to 100 K, H nuclei density 2×10^8 cm^{-3}, cosmic-ray ionization rate 3×10^{-1} s^{-1}, and assuming reactions (3b) and (4b) of Table 1. The abundance of injected ethanol and chlorine is 2.8×10^{-8} and 2.2×10^{-8}, respectively. The black dashed line shows the time used to obtain Figure 4, namely, 1500 years.

and OH, namely, rates (3b) and (4b) of Table 1. Ignoring reactions (3) and (4) results in the lowest predicted glycolaldehyde abundances. This means that the ethanol reaction with Cl plays a minor role in our model, provided that a large abundance of water is present.

Figure 5 shows the abundance of glycolaldehyde, acetic acid, formic acid, and ethanol as a function of time. In these computations, we adopted an abundance of injected ethanol and atomic chlorine equal to 2.8×10^{-8} and 2.2×10^{-8}, respectively. In the conditions assumed by the model (Section 5.1), the injected ethanol is all consumed in about 2000 years. Formic acid is the one that benefits most, followed by acetic acid, and, finally, glycolaldehyde. Before sublimated ethanol is fully consumed, the abundance ratios are $HCOOH/CH_3COOH \sim 1.5$ and $CH_3COOH/HCOCH_2OH \sim 10$, and are mostly governed by the branching ratios of the first two steps of the proposed reactions (Figure 1 and Table 1). Once ethanol is fully consumed, the relative abundance ratios are dominated by the destruction reactions (Table 3).

6. Discussion

Table 4 reports the measured abundances of ethanol, glycolaldehyde, acetic acid, and formic acid in hot corinos (NGC 1333 IRAS 4A and IRAS 2A, and IRAS 16293-2422; Jørgensen et al. 2012; Jaber et al. 2014; Coutens et al. 2015; Taquet et al. 2015) and the shocked site L1157-B1 (Lefloch et al. 2017).[14] Glycolaldehyde was also detected in two other solar-type protostars in NGC 1333 (IRAS 4B and SVS13A), with column densities similar to the ones of IRAS 4A and IRAS 2A (De Simone et al. 2017), but no measurements of ethanol, acetic acid, and/or formic acid have been reported so far.

The comparison of the model predictions with measurements of the glycolaldehyde abundance is reported in Figure 4. When considering that the predictions shown in the figure are obtained for generic hot corino conditions, the agreement with the observations is very encouraging. Obviously, the model with the reaction set (3b) and (4b) produces a larger amount of glycolaldehyde (and a lower one of formic acid and acetic acid). In addition, the scheme that we propose to synthesize glycolaldehyde from ethanol naturally explains the correlation seen by Lefloch et al. (2017) between the abundances of these two species.

On the contrary, the abundance of acetic acid and formic acid is predicted to be about one order of magnitude larger than the ones measured and reported in Table 4. We emphasize, however, that the only source in Table 4 for which there is a measurement of the formic acid abundance and an upper limit to that of acetic acid is L1157-B1, which is not a hot corino, so that a more specific modeling is necessary before firmly concluding that there is a problem. Since recent observations of two other iCOMs, acetaldehyde and formamide, in L1157-B1 show that there is segregation in their spatial distribution, we postpone such a modeling to a dedicated forthcoming article.

The other Table 4 source with an estimate of the acetic acid abundance and an upper limit to the formic acid one is IRAS 16293-2422. In this case, the discrepancy between the model predictions and the observations might suggest that important routes of destruction of the two species are missing in our network. Since we carefully checked all the "usual" ion–neutral reactions of destruction (i.e., with HCO^+, H^+, H_3^+, H_3O^+, and He^+), it is possible that major sinks are due to missing reactions involving abundant radicals. These reactions might possibly lead to an even higher degree of molecular complexity following a scheme similar to the one proposed here.

7. Conclusions

We have presented a new scheme for the synthesis of glycolaldehyde, acetic acid, and formic acid from reactions involving ethanol as an ancestor species. The initiating reactions, with H-abstraction from ethanol leading to two different reactive radicals, have been characterized in laboratory experiments (see Section 3), even though further experimental work at the relevant temperature is mandatory to determine the product branching ratios. The subsequent reactions were considered here for the first time. As there was no information on the complete chemical scheme, we have performed dedicated electronic structure and kinetics calculations to derive the rate coefficients and product branching ratios (Section 4).

The rate coefficients of the new reactions were inserted in an updated chemical network and we ran several models to predict abundances of glycolaldehyde, acetic acid, and formic acid as a function of the abundance of ethanol. The predictions compare extremely well with the measured abundance of glycolaldehyde in solar-type hot corinos and shock sites, both in terms of absolute abundance and in reproducing the correlation between the ethanol and glycolaldehyde abundances observed by Lefloch et al. (2017). Needless to say, more observations toward hot corinos are mandatory to assess the robustness of our new network of reactions leading to glycolaldehyde. The new observations and the detailed models of those sources will be able to discriminate whether the grain or gas-phase chemistry or a combination of the two are mainly responsible for glycolaldehyde formation.

On the contrary, acetic acid and formic acid are predicted to be about 10 times more abundant than the extremely sparse

[14] These observations were obtained with the single-dish telescope IRAM-30 m. Nonetheless, the abundances in Table 4 were obtained via an accurate analysis taking into account a detailed knowledge of L1157-B1.

Table 4
Abundances, with Respect to H-atoms, of Ethanol, Glycolaldehyde, Acetic Acid, and Formic Acid toward Three Hot Corinos, NGC 1333 IRAS 4A and IRAS 2A (Taquet et al. 2015), and IRAS 16293-2422 (Jørgensen et al. 2016 and Jaber et al. 2014), and the Shock Site L1157-B1 (Lefloch et al. 2017)

Source	Abundance ($\times 10^{-9}$)			
	Ethanol	Glycolaldehyde	Acetic Acid	Formic Acid
NGC 1333-IRAS 4A	2–3	0.2–6	...	...
NGC 1333-IRAS 2A	10–30	2–6	...	...
IRAS 16293-2422	2–20	0.6–2	~0.2	$\leqslant$1
L1157-B1	30–60	10–30	$\leqslant$2	7–10

detections so far available toward hot corinos and shock sites (only one in each case). This might point to a lack of important routes of destruction of these two molecules in our network, possibly via reactions involving radicals. Nonetheless, since observations are published toward only two sources and the model presented here contains a very generic description of hot corino conditions, more observations and source-dedicated modeling are necessary to confirm this discrepancy.

A more general conclusion is that the new gas-phase scheme suggested in this article increases the number of studies that show the important and previously overlooked role of neutral gas-phase chemistry in the synthesis of iCOMs. First, since the detection of iCOMs in cold prestellar objects (Bacmann et al. 2012; Cernicharo et al. 2012; Vastel et al. 2014; Jiménez-Serra et al. 2016), it has been clear that gas-phase reactions have to be relatively efficient at 10 K (Vasyunin & Herbst 2013; Balucani et al. 2015; Vasyunin et al. 2017) as the so-called warm-up phase necessary in pure grain-surface models does not take place in those objects. Second, new studies challenge the exclusive role of grain-surface chemistry in the synthesis of iCOMs also in the warm regions like hot corinos and shock sites (Barone et al. 2015; Taquet et al. 2016; Codella et al. 2017; Skouteris et al. 2017). The present study adds up new evidence that gas-phase chemistry in the iCOMs' synthesis has been overlooked, since important reactions are missing in the current astrochemistry databases.

However, the word "end" cannot be written yet, as more studies are necessary. On the one hand, observations are too scarce to draw firm conclusions, and on the other hand, more theoretical and experimental studies are needed to complete the gas-phase networks. New experimental results on neutral–neutral reactions at low T, previously disregarded because of the presence of an entrance barrier, promise to boost the role of gas-phase reactions involving radicals (Potapov et al. 2017).

We acknowledge funding from the European Research Council (ERC) in the framework of the ERC Advanced Grant Project DREAMS "Development of a Research Environment for Advanced Modeling of Soft Matter," GA No. 320951, and DOC "The Dawn of Organic Chemistry," GA No. 741002. D.S., N.B., Ce.Ce., and Cl.Co. thank Leonardo Testi, Eva Wirström, and the Gothenburg Centre for Advanced Studies in Science and Technology for the organization of the workshop Origins of Habitable Planets hosted at Chalmers (Gothenburg) in 2016 May, during which the basic ideas of this work emerged.

N.B. acknowledges the financial support from the Université Grenoble Alpes and the Observatoire de Grenoble.

This work has also been supported by MIUR "PRIN 2015" funds, project "STARS in the CAOS (Simulation Tools for Astrochemical Reactivity and Spectroscopy in the Cyberinfrastructure for Astrochemical Organic Species)," grant number 2015F59J3R.

Software: Gaussian (Frisch et al. 2013), CFOUR (http://www.cfour.de), NAHOON (http://kida.obs.u-bordeaux1.fr).

Appendix

Note 1. To the best of our knowledge, proton transfer reactions by HCO^+, H_3^+, and H_3O^+ with glycolaldehyde have not been characterized in laboratory experiments. Nevertheless, Lawson et al. (2012), who have recently characterized electron–ion recombination of protonated glycolaldehyde, have reported that glycolaldehyde is easily protonated by H_3^+ without undergoing fragmentation (differently from acetic acid and methyl formate). We have therefore attributed a rate coefficient of $2 \cdot 10^{-9}$ cm^3 s^{-1} (a rather typical value for proton transfer reactions involving large species) to the reaction with HX^+ where X = CO, H_2, H_2O.

Note 2. To the best of our knowledge, there are no laboratory characterizations of the reactions between He^+/H^+ with glycolaldehyde. Nevertheless, Cernuto et al. (2018) have recently characterized the reaction between He^+ and methyl formate, an isomer of glycolaldehyde. By far, the main ionized fragment in their experiment was found to be HCO^+. Therefore, we have associated the HCO^+ formation channel to reactions with both He^+ and H^+. In addition, since Cernuto et al. have derived a rate coefficient much smaller than the Langevin value, we have employed here a rate coefficient of $1 \cdot 10^{-9}$ cm^3 s^{-1}.

Note 3. Proton transfer reactions by HX^+ (X = CO, H_2, H_2O) with acetic acid have been characterized in laboratory experiments. There have been some indications that, after proton transfer, the protonated acetic acid dissociates. In particular, Lawson et al. (2012) claimed that it was not possible to produce protonated acetic acid without dissociation. We follow their suggestion and associate the global rate coefficient (Anicich 2003) to the formation of acetyl ion (CH_3CO^+) + H_2O + X. As for the reaction with H^+ and He^+, we have also assumed that the main channel is the formation of acetyl ion, and we have employed typical values of α for these processes.

Note 4. In the absence of any data, we have assumed that the proton transfer from HX^+ (X = CO, H_2, H_2O) is very effective for the CH_2CH_2OH/CH_3CHOH radicals (with a rate coefficient of $2 \cdot 10^{-9}$ cm^3 s^{-1}) and produces ionized ethanol (already present in the KIDA network).

Note 5. In the absence of any data, we have assumed that the interaction between CH_2CH_2OH/CH_3CHOH and H^+ causes a charge transfer producing protonated acetaldehyde. Since protonated acetaldehyde mostly recombines with an electron in a dissociative process, this assumption does not lead to

significantly different results with respect to the choice of a dissociative charge transfer (see Note 8).

Note 6. In the absence of any data, we have employed a scheme similar to the He^+ reaction with ethanol with the same rate coefficient as in the UMIST database.

Note 7. In the absence of any data, we have assumed that electron recombination of protonated glycolaldehyde produces neutral glycolaldehyde with a typical rate coefficient for this kind of process. To be noted is that significant fragmentation of glycolaldehyde can occur as already seen for other organic species (see, for instance, Hamberg et al. 2010; Vigren et al. 2013; Geppert & Larsson 2008). Therefore, the amount of glycolaldehyde produced in the model can be considered an upper limit. Since a part of glycolaldehyde is recycled back into the proton transfer/electron recombination cycle, it is necessary to quantify this effect. We will do so in a future work.

Note 8. For the dissociative electron recombination of protonated acetaldehyde we have employed the Hamberg et al. (2010) values already present in the UMIST database.

ORCID iDs

Nadia Balucani https://orcid.org/0000-0001-5121-5683
Cecilia Ceccarelli https://orcid.org/0000-0001-9664-6292
Cristina Puzzarini https://orcid.org/0000-0002-2395-8532
Claudio Codella https://orcid.org/0000-0003-1514-3074

References

Anicich, V. G. 2003, JPL Publication 03-19, An Index of the Literature for Bimolecular Gas Phase Cation-Molecule Reaction Kinetics
Bacmann, A., Taquet, V., Faure, A., Kahane, C., & Ceccarelli, C. 2012, A&A, 541, L12
Balucani, N., Ceccarelli, C., & Taquet, V. 2015, MNRAS, 449, L16
Balucani, N., Skouteris, D., Leonori, F., et al. 2012, JPCA, 116, 10467
Barone, V., Latouche, C., Skouteris, D., et al. 2015, MNRAS, 453, L31
Béltran, M. T., Codella, C., Viti, S., Neri, R., & Cesaroni, R. 2009, ApJL, 690, L93
Bergantini, A., Maksyutenko, P., & Kaiser, R. I. 2017, ApJ, 841, 96
Boogert, A. C. A., Gerakines, P. A., & Whittet, D. C. B. 2015, ARA&A, 53, 541
Butscher, T., Duvernay, F., Danger, G., et al. 2016, A&A, 593, A60
Butscher, T., Duvernay, F., Theule, P., et al. 2015, MNRAS, 453, 1587
Caravan, R. L., Shannon, R. J., Lewis, T., Blitz, M. A., & Heard, D. E. 2015, JPCA, 119, 7130
Carr, S. A., Blitz, M. A., & Seakins, P. W. 2011, JPCA, 115, 3335
Caselli, P., & Ceccarelli, C. 2012, A&ARv, 20, 56
Ceccarelli, C., Caselli, P., Fontani, F., et al. 2017, ApJ, 850, 176
Cernicharo, J., Marcelino, N., Roueff, E., et al. 2012, ApJ, 759, 43
Cernuto, A., Pirani, F., Martini, L. M., Tosi, P., & Ascenzi, D. 2018, ChemPhysChem, 19, 51
Charnley, S. B. 2004, AdSpR, 33, 23
Chuang, K.-J., Fedoseev, G., Qasim, D., et al. 2017, MNRAS, 467, 2552
Codella, C., Ceccarelli, C., Bottinelli, et al. 2012, ApJL, 744, L164
Codella, C., Ceccarelli, C., Caselli, P., et al. 2017, A&A, 605, L3
Codella, C., Fontani, F., Ceccarelli, C., et al. 2015, MNRAS, 449, L11
Coutens, A., Jorgensen, J. K., van der Wiel, M. H. D., et al. 2016, A&A, 590, L6
Coutens, A., Jørgensen, J. K., Wampfler, S. F., & Lykke, J. M. 2015, A&A, 576, 5
De Simone, M., Codella, C., Testi, L., et al. 2017, A&A, 599, 121
Dunning, T. H. 1989, JChPh, 90, 1007
Edelbüttel-Einhaus, J., Hoyermann, K., Rohde, G., & Seeba, J. 1992, in Proc. XXIV Symp. (Int.) on Combustion (Pittsburgh, PA: Combustion Institute), 661
Enrique-Romero, J., Rimola, A., Ceccarelli, C., & Balucani, N. 2016, MNRAS, 459, L6
Fedoseev, G., Cuppen, H. M., Ioppolo, S., Lamberts, T., & Linnartz, H. 2015, MNRAS, 448, 1288
Frisch, M. J., Trucks, G. W., Schlegel, H. B., et al. 2013, Gaussian09 GDVH32
Garrod, R. T., & Herbst, E. 2006, A&A, 457, 927
Garrod, R. T., Weaver, S. L. W., & Herbst, E. 2008, ApJ, 682, 283
Geppert, W. D., & Larsson, M. 2008, MolPh, 106, 2199
Goerigk, L., & Grimme, S. 2011, J. Chem. Theory Comput., 7, 291
Grimme, S., Ehrlich, S., & Goerigk, L. 2011, J. Comput. Chem., 32, 1456
Grimme, S. J. 2006, Chem. Phys., 124, 034108
Halfen, D. T., Apponi, A. J., Woolf, N., et al. 2006, ApJ, 639, 237
Hamberg, M., Zhaunerchyk, V., Vigren, E., et al. 2010, A&A, 522, A90
Heckert, M., Kállay, M., & Gauss, J. 2005, MolPh, 103, 2109
Heckert, M., Kállay, M., Tew, D. P., Klopper, W., & Gauss, J. 2006, JChPh, 125, 044108
Herbst, E. 1985, ApJ, 291, 226
Hollis, J. M., Lovas, F. J., & Jewell, P. R. 2000, ApJL, 540, L107
Horn, A., Møllendal, H., Sekiguchi, O., et al. 2004, ApJ, 611, 605
Jaber, A., Ceccarelli, C., Kahane, C., & Caux, E. 2014, ApJ, 791, 29
Jalbout, A. F. 2007, MolPh, 105, 941
Jenkins, E. B. 2009, ApJ, 700, 1299
Jiménez-Serra, I., Vasyunin, A., Caselli, P., et al. 2016, ApJL, 830, L6
Jørgensen, J. K., Favre, C., Bisschop, S., et al. 2012, ApJL, 757, L4
Jørgensen, J. K., van der Wiel, M. H., Coutens, A., et al. 2016, A&A, 595, 117
Kahane, C., Ceccarelli, C., Faure, A., & Caux, E. 2013, ApJL, 763, L38
Kama, M., Caux, E., López-Sepulcre, et al. 2015, A&A, 574, 107
Karpas, Z., & Klein, F. S. 1975, IJMSI, 18, 65
Lawson, P. A., Osborne, D. S., Jr., & Adams, N. G. 2012, JPCA, 116, 2880
Lefloch, B., Ceccarelli, C., Codella, C., et al. 2017, MNRAS, 469, L73
Leonori, F., Skouteris, D., Petrucci, R., et al. 2013, JChPh, 138, 024311
Loison, J.-C., Wakelam, V., Hickson, K., et al. 2014, MNRAS, 443, 398
Maity, S., Kaiser, R., & Jones, B. M. 2014, FaDi, 168, 485
Marinov, N. M. 1999, Int J Chem Kinet., 31, 183
McElroy, D., Walsh, C., Markwick, A. J., et al. 2013, A&A, 550, A36
Neufeld, D. A., Roueff, E., Snell, R. L., et al. 2012, ApJ, 748, 37
Oberg, K. I., Boogert, A. C. A., Pontoppidan, K. M., et al. 2011, ApJ, 740, 109
Papajak, E., Leverentz, H. R., Zheng, J., & Truhlar, D. G. 2009, J. Chem. Theory Comput., 5, 1197
Peng, R., Yoshida, H., Chamberlin, R. A., et al. 2010, ApJ, 723, 218
Potapov, A., Canosa, A., Jiménez, E., et al. 2017, Angew. Chem. Int. Ed., 56, 8618
Raghavachari, K., Trucks, G. W., Pople, J. A., & Head-Gordon, M. 1989, CPL, 157, 479
Rimola, A., Skouteris, D., Balucani, N., et al. 2017, ACS Earth Space Chem., submitted
Ruaud, M., Wakelam, V., & Hersant, F. 2016, MNRAS, 459, 3756
Rubin, R. H., Swenson, G. W., Jr., Benson, R. C., Tigelaar, H. L., & Flygare, W. H. 1971, ApJL, 169, L39
Rudic, S., Murray, C., Ascenzi, D., et al. 2002, JChPh, 117, 5692
Rusic, B., & Berkowitz, J. 1994, JChPh, 101, 10936
Schutte, W. A., Boogert, A. C. A., Tielens, A. G. G. M., et al. 1999, A&A, 343, 966
Shannon, R. J., Blitz, M. A., Goddard, A., & Heard, D. E. 2013, NatCh, 5, 745
Shannon, R. J., Caravan, R. L., Blitz, M. A., & Heard, D. E. 2014, PCCP, 16, 3466
Skouteris, D., Balucani, N., Faginas-Lago, N., Falcinelli, S., & Rosi, M. 2015, A&A, 584, 76
Skouteris, D., Vazart, F., Ceccarelli, C., et al. 2017, MNRAS, 468, L1
Sleiman, C., El Dib, G., Rosi, M., et al. 2017, PCCP, 2018, doi:10.1039/C7CP05746F
Song, L., & Kästner, J. 2016, PCCP, 18, 29278
Spezia, R., Jeanvoine, Y., Hase, W. L., Song, K., & Largo, A. 2016, ApJ, 826, 107
Taatjes, C. A., Christensen, L. K., Hurley, M. D., & Wallington, T. J. 1999, JPCA, 103, 9805
Taquet, V., López-Sepulcre, A., Ceccarelli, C., et al. 2015, ApJ, 804, 81
Vastel, C., Ceccarelli, C., Lefloch, B., & Bachiller, R. 2014, ApJL, 795, L2
Vasyunin, A., & Herbst, E. 2013, ApJ, 769, 34
Vasyunin, A. I., Caselli, P., Dulieu, F., & Jiménez-Serra, I. 2017, ApJ, 842, 33
Vazart, F., Calderini, D., Puzzarini, C., et al. 2016, J. Chem. Theory Comput., 12, 5385
Vazart, F., Latouche, C., Skouteris, D., Balucani, N., & Barone, V. 2015, ApJ, 810, 2
Vigren, E., Hamberg, M., Zhaunerchyk, V., et al. 2013, ApJ, 709, 1429
Wakelam, V. 2014, Nahoon: Time-dependent Gas-phase Chemical Model, Astrophysics Source Code Library, ascl:1409.009
Wakelam, V., Loison, J.-C., Herbst, E., et al. 2015, ApJS, 217, 20
Wang, T., & Bowie, J. H. 2010, Org. Biomol. Chem., 8, 4757
Woods, P. M., Kelly, G., & Viti, S. 2012, ApJ, 750, 19
Woods, P. M., Slater, B., Raza, Z., et al. 2013, ApJ, 777, 90
Woon, D. E., & Dunning, T. H., Jr. 1995, JChPh, 103, 4572
Xu, S., & Lin, M. C. 2007, Proc. of the Combustion Inst., 31, 159